

Quantum Monte Carlo simulations of fidelity at magnetic quantum phase transitions

David Schwandt,^{1,2} Fabien Alet,^{1,2} and Sylvain Capponi^{1,2}

¹Laboratoire de Physique Théorique, Université de Toulouse, UPS, (IRSAMC), F-31062 Toulouse, France

²CNRS, LPT (IRSAMC), F-31062 Toulouse, France

(Dated: October 30, 2018)

When a system undergoes a quantum phase transition, the ground-state wave-function shows a change of nature, which can be monitored using the *fidelity* concept. We introduce two Quantum Monte Carlo schemes that allow the computation of fidelity and its susceptibility for large interacting many-body systems. These methods are illustrated on a two-dimensional Heisenberg model, where fidelity estimators show marked behaviours at two successive quantum phase transitions. We also develop a scaling theory which relates the divergence of the fidelity susceptibility to the critical exponent of the correlation length. A good agreement is found with the numerical results.

PACS numbers: 03.67.-a, 02.70.Ss, 64.70.Tg, 75.10.Jm

What happens to the ground-state (GS) wave-function when a physical system goes across a quantum phase transition (QPT)? Rooted in quantum information theory, the fidelity approach [1, 2] provides an interesting global answer in terms of the overlap between GS of the system at two different values of the driving parameter. The basic idea, which precursor may be found in Anderson's orthogonality catastrophe [3], is that close quantum states become more orthogonal close to a phase transition. The resulting fidelity drop can then provide a useful probe to detect the QPT. This is particularly interesting as the fidelity is a global, model-independent quantity that incorporates all the information contained in the GS wave-functions. This is opposite to other usual approaches to phase transitions, which often need an input such as the knowledge of a specific order parameter.

Consider the Hamiltonian

$$H = H_0 + \lambda H_\lambda \quad (1)$$

with H_λ acting as a perturbation to H_0 . The fidelity $F(\lambda_1, \lambda_2)$ is defined as the modulus of the overlap between GS of H at two different values of λ :

$$F(\lambda_1, \lambda_2) = |\langle \psi_0^{\lambda_1} | \psi_0^{\lambda_2} \rangle|.$$

Suppose that the system undergoes a QPT for a value λ_c of the driving parameter. We expect the fidelity to have a singular behaviour when either λ_1 or λ_2 are close to λ_c , especially if the difference $\delta\lambda = \lambda_2 - \lambda_1$ is small [1]. When $\delta\lambda \rightarrow 0$, the fidelity is dominated by its leading term, the fidelity susceptibility χ_F [4], with $F \simeq 1 - \frac{\delta\lambda^2}{2} \chi_F$.

When H describes a many-body system, computations of F or χ_F are complicated. Besides a few analytical results on specific models [2], the main effort has been put in their numerical evaluation. Exact diagonalization (ED) and tensor-network (TN) methods [5] -including density matrix renormalization group (DMRG) [6]- have been the most widely used techniques in that respect, even though they suffer from several caveats. The ED method needs the full computation of the GS wave-function and is therefore limited to small systems. TN

methods provide a variational ansatz for the GS wave-functions, allowing a straightforward computation of overlaps. This ansatz turns out to be excellent for one-dimensional systems, where DMRG [6] in particular has proved its full strength. Recently, several TN based works studied two-dimensional ($2d$) systems and their fidelity properties [7]. However, these methods remain variational and may fail in correctly capturing the GS properties of complex many-body Hamiltonians in $d > 1$, especially close to a QPT.

In this Letter, we present two different Quantum Monte Carlo (QMC) schemes which allow an *exact* (albeit stochastic) computation of the fidelity F and its susceptibility χ_F . We apply these methods to the antiferromagnetic (AF) Heisenberg spin model on a $2d$ lattice. Varying one exchange coupling in the spin model causes two successive phase transitions, both of which are found to be captured by the fidelity and its susceptibility. In passing, we derive a scaling theory for the divergence of χ_F at a second-order QPT. The two schemes benefit from the power of QMC methods, which allow to treat very large systems *in any dimension*. The first scheme, which calculates F , is applicable to all AF systems admitting a singlet GS. The second scheme for χ_F is even more general and can be applied to several many-body problems. This opens a novel path for the fidelity approach to QPT. These techniques are only efficient when the underlying QMC method is, *i.e.* when there is no sign problem.

Model — The schemes are illustrated on the spin-1/2 Heisenberg Hamiltonian

$$H = H_0 + \lambda H_\lambda = \sum_{\langle ij \rangle_0} \mathbf{S}_i \cdot \mathbf{S}_j + \lambda \sum_{\langle ij \rangle_\lambda} \mathbf{S}_i \cdot \mathbf{S}_j \quad (2)$$

on the CaVO lattice [8], a 1/5th depleted square lattice (see Fig. 1). The first sum runs over nearest-neighbor spins on 0-bonds (solid lines in Fig. 1) while the second is over λ -bonds (dashed lines). This lattice structure can be found in the AF compound CaV_4O_9 (hence the lattice name), even though the interactions are more complex in

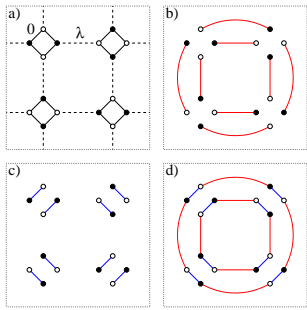


FIG. 1: (color online) (a) CaVO lattice with nearest neighbor bonds of type λ (dashed lines) and 0 (solid lines). (b)-(c) Typical VB states on the CaVO lattice. (d) Overlap graph of previous VB states forming two loops.

the real compound [9]. Varying the coupling λ allows the occurrence of two QPT separating an intermediate Néel-ordered AF phase from respectively a low- λ plaquette and a high- λ dimer phase [8, 10]. H conserves the total spin of the system and in particular, AF interactions $\lambda > 0$ lead to a singlet GS.

Fidelity measurements — Measuring the fidelity seems at first glance easy within a standard Projection QMC scheme [11]. Decomposing the ground-state $|\psi_0^\lambda\rangle = \sum_i a_i |\varphi_i^\lambda\rangle$ in the simulation basis $\{|\varphi\rangle\}$, one generates representatives $|\varphi_i^\lambda\rangle$ (*i.e.* in proportion of $|a_i\rangle$) of the GS via the projection scheme for two different values of λ . The problem comes from the fact that the QMC estimate of the fidelity $\langle \varphi_i^{\lambda_1} | \varphi_i^{\lambda_2} \rangle$ will vanish most of the time in the commonly used orthogonal basis, leading to a serious statistical problem. However, when the GS is a singlet, it can be decomposed in the Valence Bond (VB) basis, which has a crucial non-orthogonality property. Indeed, any two VB states always have a non-zero fidelity $F = |\langle \varphi_1 | \varphi_2 \rangle| = 2^{N_\ell - N/2}$ where N_ℓ is the number of loops obtained by superimposing the two VB states (see Fig. 1), and N the total number of spins. This property solves the statistical problem and allows an efficient computation of the fidelity.

More specifically, we work with a VB projector loop algorithm recently proposed by Sandvik and Evertz [12]. To avoid the sign problem, we simulate non-frustrated AF on bipartite lattices, which leads to real positive values of coefficients $a_i \geq 0$ and of VB overlaps $\langle \varphi_1 | \varphi_2 \rangle > 0$. In the VB loop algorithm [12], two VB representatives $|\varphi_L\rangle$ and $|\varphi_R\rangle$ of the ground-state are generated by propagating two initial VB states. Simulating at the same time *two* different physical systems with couplings λ_1 and λ_2 allows a QMC estimator of the square of the fidelity:

$$F^2(\lambda_1, \lambda_2) = \frac{\langle \varphi_L^{\lambda_1} | \varphi_R^{\lambda_2} \rangle \langle \varphi_R^{\lambda_1} | \varphi_L^{\lambda_2} \rangle}{\langle \varphi_L^{\lambda_1} | \varphi_R^{\lambda_1} \rangle \langle \varphi_L^{\lambda_2} | \varphi_R^{\lambda_2} \rangle}.$$

$F(\lambda_1, \lambda_2)$ can be computed for any value of λ_1 and λ_2 for all models that can be simulated with VB QMC methods.

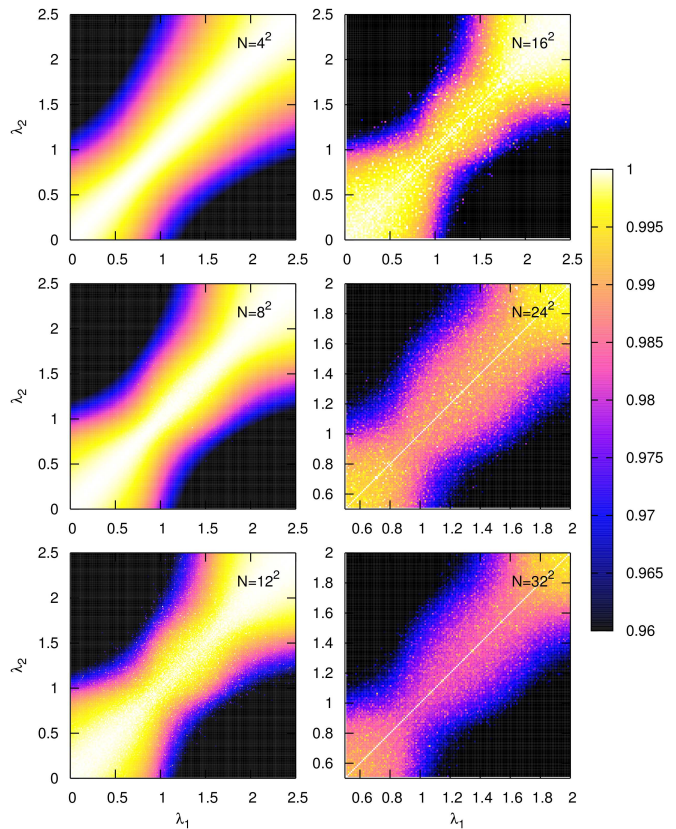


FIG. 2: (color online) Fidelity per site f as function of λ_1 and λ_2 for different system sizes. Expansion power n of H in the VB QMC method is $n/N = 20$ for $N \leq 12^2$, 10 for $N \leq 16^2$ and 4 for $N \geq 24^2$. λ range is $[0, 2.5]$ for $N \leq 16^2$ and $[0.5, 2]$ for $N \geq 24^2$. Resolution $\Delta\lambda$ for the plots is 0.02 for $N = 16^2$, 0.01 otherwise.

In the following, we illustrate this method for the Heisenberg model on the CaVO lattice (Eq. 2). The unit cell contains 4 spins, and we simulated square samples with $L \times L$ unit cells (total number of spins $N = 4L^2$) up to $L = 16$, using periodic boundary conditions. For such large systems, the fidelity essentially vanishes for all $\lambda_1 \neq \lambda_2$. As suggested in Ref. [13], we compute the fidelity per site $f(\lambda_1, \lambda_2) = F(\lambda_1, \lambda_2)^{1/N}$, which is well-behaved as $N \rightarrow \infty$.

Our data for the fidelity per site are presented on Fig. 2. Around the diagonal where $f(\lambda, \lambda) = 1$, we notice the appearance of two pinch points, roughly around $\lambda_c^1 \in [0.8, 1.1]$ and $\lambda_c^2 \in [1.5, 1.8]$. It has been argued that these features are characteristic of continuous QPT [13] and our results are in agreement with the two well-known second-order QPT in this model. Far enough away from these two critical regions we notice that there is no significant change of f when $N \rightarrow \infty$. Within the critical regions f drops faster with system size. Given our statistical errors (up to 2% for the chosen range of λ), we cannot however provide more precise ranges for the crit-

ical points. To locate more accurately the QPT, we now turn to the leading correction of fidelity around the diagonal $\lambda_1 = \lambda_2$.

Fidelity susceptibility — For $\delta\lambda \rightarrow 0$, we consider the fidelity susceptibility χ_F which can be expressed [4] as the imaginary-time integral $\chi_F = \int_0^\infty \tau [\langle H_\lambda(0)H_\lambda(\tau) \rangle - \langle H_\lambda(0) \rangle^2] d\tau$. This definition offers a natural extension to finite temperature $T = 1/\beta$:

$$\chi_F(\beta) = \int_0^{\beta/2} \tau [\langle H_\lambda(0)H_\lambda(\tau) \rangle - \langle H_\lambda(0) \rangle^2] d\tau. \quad (3)$$

and $\chi_F = \lim_{\beta \rightarrow \infty} \chi_F(\beta)$. This definition of $\chi_F(\beta)$ differs from the Bures metric ds^2 usually defined for mixed states [14], even though both have the same $T = 0$ limit. However, one can prove [15] that $ds^2/2 \leq \chi_F(\beta) \leq ds^2$, showing that both quantities scale in the same way.

An advantage of Eq. (3) is that $\chi_F(\beta)$ can be computed within a QMC stochastic series expansion (SSE) formalism [16, 17]. Note the importance of taking $\beta/2$ as the upper limit of the integral as the β -periodicity of the path integral would lead otherwise to incorrect results. In the SSE formalism the partition function is expanded in powers of β , $Z = \sum_{n=0}^\infty \frac{(-\beta)^n}{n!} \text{Tr} H^n$. Starting from the expression of time-displaced correlations functions in SSE (Eq. 3.15 of Ref. 16), $\chi_F(\beta)$ is estimated as

$$\chi_F(\beta) = \frac{1}{\lambda^2} \left[\sum_{m=0}^{n-2} A(m, n) \langle N_\lambda(m) \rangle - \langle N_\lambda \rangle^2 / 8 \right] \quad (4)$$

where $N_\lambda(m)$ is the number of times two elements of H_λ appear separated by m positions in the SSE sequence [16] and N_λ the total number of appearance of elements of H_λ . The amplitude $A(m, n) = \frac{(n-1)!}{(n-m-2)!m!} \int_0^{1/2} d\tau \tau^{m+1} (1-\tau)^{n-m-2}$ can be calculated for all (m, n) prior to simulations by numerical integration or analytically for large n [15]. We emphasize that this formalism allows to compute $\chi_F(\beta)$ for any model which can be simulated with SSE.

The computation of $\chi_F(\beta)$ can turn costly for large systems at low T . We reached $L \leq 16$ and used $\beta = 10L$ for the CaVO lattice, and limited simulations to the relevant λ range for the largest L and β .

Fig. 3(a)-(f) display the susceptibility fidelity per site χ_F/N , showing the apparition of two peaks as a function of λ . While the $N = 4^2$ and 8^2 samples show rather broad feature (especially for the second peak), the peaks are clearly emergent as system size is increased and temperature lowered. From the position of the two peaks for the lowest T and largest size, one obtains estimates $\lambda_c^1 = 0.94(1)$ and $\lambda_c^2 = 1.65(1)$ for the two quantum critical points, in full agreement with QMC computations of order parameter and spin gap [10]. Note that the positions of the maxima of χ_F at finite T (see Fig. 3(e)-(f)) also allow to determine faithfully λ_c^1 and λ_c^2 , even though a small shift is observed if β is too low. We therefore find

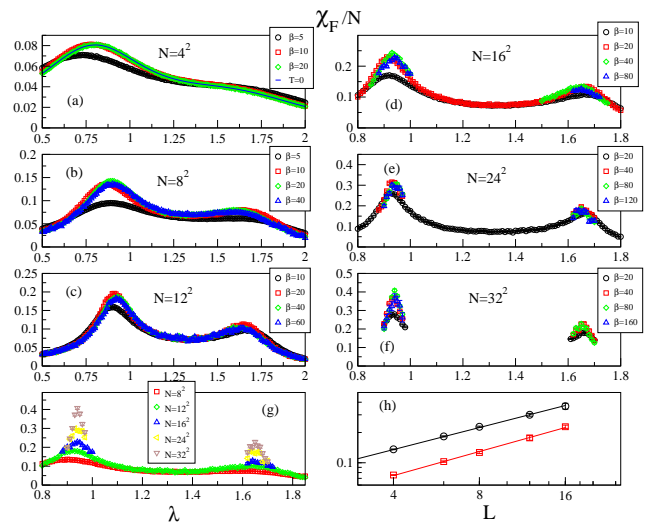


FIG. 3: (color online) (a)-(f) Fidelity susceptibility per site χ_F/N versus λ for different system sizes N and inverse temperature β . (g) χ_F/N versus λ for the largest β for different N . (h) Scaling of the two peaks of χ_F/N versus linear size L (log-log scale). Lines denote power-law fits.

that the fidelity susceptibility behaves as a good global indicator of QPTs in a $2d$ quantum system.

Away from criticality, χ_F is extensive in all phases - see Fig. 3(g). Scaling of the peaks in Fig. 3(h) reveals a power-law divergence at criticality $\chi_F(\lambda_c)/N \sim L^\omega$, with $\omega = 0.73(3)$ for the first QPT and $\omega = 0.79(6)$ for the second (error bars originate from the statistical error bar in the QMC data). This agrees with the behaviour of f which develops pinch points at criticality but essentially does not change in non-critical regions as $N \rightarrow \infty$. The observed symmetry of the peaks around their divergence explains the hourglass shape of the pinch points in f . We also understand why the second pinch point is harder to see in Fig. 2: indeed χ_F is much smaller close to λ_c^2 than to λ_c^1 (almost a factor of 2 in all cases).

Scaling theory — We now account for the divergence at the QPT by formulating a finite-size scaling (FSS) theory. FSS theories for χ_F have been proposed earlier but the relation to standard critical exponents at second-order QPT has been missed. In the most elaborate work, Campos Venuti and Zanardi [18] discuss the divergence of χ_F as a function of the scaling dimension $[H_\lambda]$ of the part of the Hamiltonian that drives the transition, *i.e.* how this operator scales at λ_c : $H_\lambda \sim L^{-[H_\lambda]}$. Here we explicitly calculate this scaling dimension. From the definition of the correlation length critical exponent $\xi \sim (\lambda - \lambda_c)^{-\nu}$, we have $[\lambda] = 1/\nu$. Noting that $[H] = z$ where z is the dynamical critical exponent, we deduce $[H_\lambda] = z - 1/\nu$ from Eq. (1). Finally, we conclude from Eq. (3) that $[\chi_F] = 2[\tau] + 2[H_\lambda] = -2/\nu$ (see also Ref. [18]) and there-

fore $[\chi_F/N] = -2/\nu + d$, leading to the prediction:

$$\chi_F(\lambda_c)/N \sim L^{2/\nu-d}. \quad (5)$$

This relation should hold for all second-order QPT and explains the superextensive behaviour generally observed for χ_F in terms of the usual critical exponents. From the value $\nu \simeq 0.7112$ of the universality class of the 3d $O(3)$ model [19] to which belong both QPT studied here, we expect from this analysis $\omega \simeq 0.812$, in agreement with our numerical estimates.

Discussions and conclusion — In conclusion, we presented two QMC schemes that are able to calculate with high accuracy the fidelity and its susceptibility for quantum interacting systems, in any dimension. This allows to pin down the behaviour of fidelity at QPT, using one of the most sophisticated numerical techniques for the many-body problem. Taking the example of the Heisenberg model on the CaVO lattice, we find that both F and χ_F are able to locate the two quantum critical points present in this system. The fidelity susceptibility acts as a more precise indicator as criticality manifests itself as a marked peak in χ_F . However, there is in principle more information contained in F . This could be useful to detect transitions that χ_F does not capture [20], as well as in the context of quantum quenches [21, 22].

The divergence of χ_F at criticality is accounted for by the scaling theory that we have presented, where the connection to the correlation length exponent of the universality class of the QPT is made. We also showed that the generalization of χ_F to finite temperature (Eq. 3) allows to detect criticality for moderate values of T . This is of practical interest as simulations can be performed at a smaller computational cost.

The method proposed for measuring χ_F works for any model which can be simulated within the generic SSE scheme [16, 17], opening the door to the study of fidelity in many different physical systems. We expect that our scheme can be extended to measure the Loschmidt echo, another witness of quantum criticality [23], which can be measured experimentally in this context [24].

Note added — The scaling relation Eq. (5) has been independently derived in recent preprints [22].

Acknowledgments — We thank F. Albuquerque, A. Läuchli, O. Motrunich, G. Roux and C. Sire for very useful discussions. Calculations were performed using the ALPS libraries [25]. We thank GENCI and CALMIP for allocation of CPU time. This work is supported by the French ANR program ANR-08-JCJC-0056-01.

-
- [1] P. Zanardi and N. Paunković, Phys. Rev. E **74**, 031123 (2006); P. Zanardi, P. Giorda and M. Cozzini, Phys. Rev. Lett. **99**, 100603 (2007).
 - [2] For a review, see S.-J. Gu, arXiv:0811.3127.
 - [3] P.W. Anderson, Phys. Rev. Lett. **18**, 1049 (1967).
 - [4] W.-L. You, Y.-W. Li and S.-J. Gu, Phys. Rev. E **76**, 022101 (2007).
 - [5] For a review, see F. Verstraete, V. Murg and J.I. Cirac, Adv. Phys. **57**, 143 (2007). Recent advances include J. Jordan *et al.*, Phys. Rev. Lett. **101**, 250602 (2008); H.-C. Jiang, Z.-Y. Weng and T. Xiang, *ibid* **101**, 090603 (2008); R. Orús, A.C. Doherty and G. Vidal, *ibid* **102** 077203 (2009); Z.-C. Gu, M. Levin and X.-G. Wen, Phys. Rev. B **78**, 205116 (2008).
 - [6] S.R. White, Phys. Rev. Lett. **69**, 2863 (1992).
 - [7] H.-Q. Zhou, R. Orús and G. Vidal, Phys. Rev. Lett. **100**, 080601 (2008); B. Li, S.-H. Li and H.-Q. Zhou, Phys. Rev. E **79**, 060101(R) (2009); J. Jordan, R. Orús and G. Vidal, Phys. Rev. B **79**, 174515 (2009).
 - [8] K. Ueda *et al.*, Phys. Rev. Lett. **76**, 1932 (1996).
 - [9] K. Kodama, J. Phys. Soc. Jpn. **66**, 793 (1997); M.A. Korotin *et al.*, Phys. Rev. Lett. **83**, 1387 (1999).
 - [10] M. Troyer, H. Kontani, and K. Ueda, Phys. Rev. Lett. **76**, 3822 (1996); M. Troyer, M. Imada and K. Ueda, J. Phys. Soc. Jpn. **66**, 2957 (1997).
 - [11] N. Trivedi and D.M. Ceperley, Phys. Rev. B **40**, 2737 (1989).
 - [12] A.W. Sandvik and H.G. Evertz, arXiv:0807.0682.
 - [13] H.-Q. Zhou and J.-P. Barjaktarevic, J. Phys. A **41**, 412001 (2008); H.-Q. Zhou, J.-H. Zhao and B. Li, *ibid* **41**, 492002 (2008).
 - [14] P. Zanardi, L. Campos Venuti and P. Giorda, Phys. Rev. A **76**, 062318 (2007).
 - [15] F. Albuquerque *et al.*, in preparation.
 - [16] A.W. Sandvik, J. Phys. A **25**, 3667 (1992).
 - [17] A.W. Sandvik, Phys. Rev. B **59**, R14157 (1999).
 - [18] L. Campos Venuti and P. Zanardi, Phys. Rev. Lett. **99**, 095701 (2007).
 - [19] M. Campostrini *et al.*, Phys. Rev. B **65**, 144520 (2002).
 - [20] Y.-C. Tzeng *et al.*, Phys. Rev. A **77**, 062321 (2008).
 - [21] A. Peres, Phys. Rev. A **30**, 1610 (1984); G. Roux, arXiv:0909.4620
 - [22] C. De Grandi, V. Gritsev and A. Polkovnikov, arXiv:0909.5181, arXiv:0910.0876; R. Barankov, arXiv:0910.0255
 - [23] H. T. Quan *et al.*, Phys. Rev. Lett. **96**, 140604 (2006).
 - [24] J. Zhang *et al.*, Phys. Rev. A **79**, 012305 (2009).
 - [25] F. Albuquerque *et al.*, J. Magn. Magn. Mater. **310**, 1187 (2007); M. Troyer, B. Ammon and E. Heeb, Lecture Notes in Comput. Sci., **1505**, 191 (1998); F. Alet, S. Wessel and M. Troyer, Phys. Rev. E **71**, 036706 (2005); see <http://alps.comp-phys.org>.